

SUMMARY OF HTS WORK AT TD

E. Barzi, D. Turrioni, V. Lombardo, A. Kikuchi (NIMS), M. Lamm, R. Yamada,
A. Zlobin

With:

H. Miao, S. Hong (OST)

K. Marken (LANL)

C. Thieme (AMSC)

ABSTRACT

The experiment, which is in the works at FNAL to confirm that ionization cooling is an efficient way to shrink the size of a muon beam, would pave the way for Muon Collider machines, which require in their last stages of cooling and of acceleration very high field (> 25 T) solenoids. Two kinds of high temperature superconducting materials (HTS) are being considered for these magnets:

- $\text{Bi}_2\text{Sr}_2\text{CaCu}_2\text{O}_{8-x}$ (BSCCO-2212) as a round multifilamentary wire, which can be cabled in the form of Rutherford-type cables.
- Anisotropic conductors, including $(\text{Bi,Pb})_2\text{Sr}_2\text{Ca}_2\text{Cu}_3\text{O}_x$ (BSCCO-2223) and second generation coated conductors (YBCO).

The conductor program focuses on the following important issues:

- Monitoring state-of-the-art HTS's and keep all options open.
- Understand field and temperature dependence of anisotropy in tapes.
- Solve the powder leak problem in Bi-2212.
- Develop appropriate cable and coil technologies.

INTRODUCTION

The continued progress toward higher magnetic fields holds significant potential for general advances in science and technology [1]. For the past twenty years there have been steady increases in the field strength of superconducting magnets due to continued advances in Nb_3Sn conductor and magnet technology [2, 3]. The most recent internal tin Nb_3Sn conductors have enabled a commercial 22.3 T magnet for 950 MHz NMR spectroscopy [4, 5]. While Nb_3Sn can possibly enable 23.5 T for 1 GHz NMR, it is quite unlikely that this material can enable fields above 25 T. For the R&D on the solenoids required in the last stages of cooling and acceleration of muon

collider machines, HTS are an option to explore. Below is a description of the work performed recently at TD on these materials.

To enable cabling of Bi-2212 round stands, for this work OST produced billets with different O₂ anneal processes. Those that passed the bending test were used to fabricate a number (nine) of Rutherford-type cables at FNAL. Virgin (round) strands, strands extracted from each cable and cable samples with welded ends were heat treated in Oxygen at OST, and tested in Helium at FNAL, where surface EDS/SEM analysis was also performed [6].

Because of the perpendicular field components in solenoid end sections and the anisotropic nature of these conductors, it is important to know their I_c angular dependence. For this purpose, a sample holder for HTS tests in a B-I degree range of 0 to 90 was designed, procured, and commissioned. This allows testing HTS tapes between 1.8 K and 77 K up to 15 T, while providing up to 1800 A of current [7].

BSCCO-2212 WIRE AND CABLE STUDIES

Bi₂Sr₂CaCu₂O_{8-x} (BSCCO-2212) is one of a large number of copper-oxide high temperature superconductors (HTS), which in addition to much higher critical temperatures also have very high critical fields compared with LTS [8, 9]. However BSCCO-2212 is the only copper oxide material which can be easily melt processed, which enables it to be fabricated in a wide variety of shapes, including conventional round multifilamentary wire. Some tens of kilometers of 2212 wire have been cabled, most of it coming from Showa Electric Wire Company in Japan [10, 11]. Several cabling trials have been made using OST's 2212 wire, the earliest being among the first made from this material [12].

The OST wire fabrication process uses a Ag0.2%Mg alloy sheath which is dispersion strengthened by oxidation of the Mg during heat treatment [13]. The best performance is usually obtained by oxygen preannealing of the AgMg sheathed strand. However, the hardened sheath which results from this preanneal severely restricts the diameter around which the wire can be bent without cracking. To enable cabling of Bi-2212 round stands, for this work OST produced billets with different O₂ anneal processes. Those that passed the bending test were used to fabricate a number of Rutherford-type cables. Samples were heat treated at OST according to an optimized schedule. The transport performance at 4.2 K of round and extracted strands was measured up to 15 T, and a number of cables were tested at self-field. To better explain the results, SEM/EDS analysis was also performed.

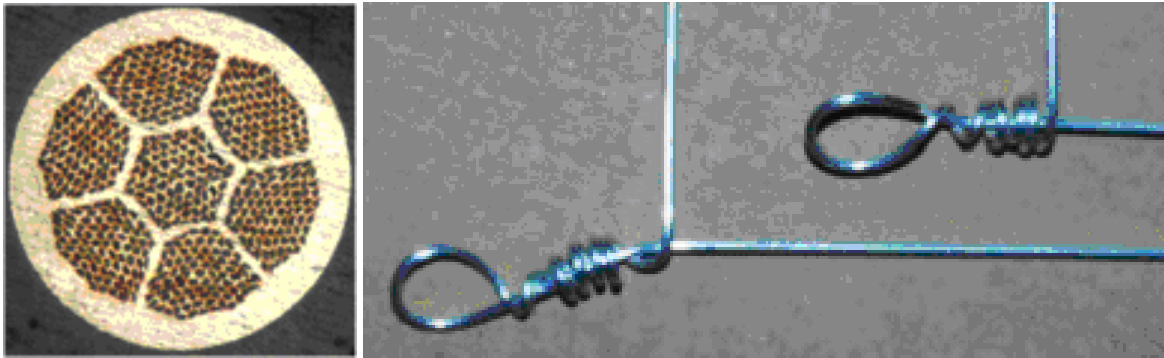
EXPERIMENTAL SETUP

Strand Description

The 2212 strands that were studied are described in Table 1, and a cross section is shown in Figure 1 (left). Strands A, B, and D passed the bending test, as shown in Figure 1 (right, top right corner), and were therefore used for cabling.

TABLE 1. Strand Description

Strand ID	Billet No.	Diameter, mm	Total length, m	Fill factor, %	Peak J _c , A/mm ²	Peak J _E , A/mm ²	Passed bending test
A	PMM050518	1.02	248	22.3	-	-	Y
B	PMM050419	0.81	371	22.4	-	-	Y
C	PMM060505	0.7, 0.81, 0.9	357	28.2	4070	1148	N
D	PMM060508-1	0.7, 0.81, 0.91	360	26.4	3678	971	Y

**FIGURE 1.** BSCCO-2212 strand cross section (left), and), and examples of unsuccessful (right, bottom left corner) and successful (right, top right corner) bending test.

Cable Parameters

The cables were all rectangular and made in one pass. They were fabricated at FNAL using the same mandrel and a forming fixture made of two vertical rolls with variable gap, and of two thin horizontal rolls [14]. About 40 meters of cable were made, producing nine samples with packing factors (PF) ranging between 81% and ~87%. This was done by varying the cable mean thickness. The lay angle of all cables was 14°. Table 2 details the cable parameters, and Figure 2 shows some cross sections. In a couple of cases (cables 7 and 8) the cable map included different strands (see Table 2) to comply with lack of material.

TABLE 2. Cable Description

Cable ID	No. strands	Strand size, mm	Strands used	Ave. thickness, mm	Average width, mm	PF, %	Tested
1	19	1.02	A	1.938 ±0.003	9.992 ±0.050	82.6	Y
2	“	“	“	1.883 ±0.007	9.987 ±0.031	85.1	N
3	“	“	“	1.848 ±0.009	10.008 ±0.022	86.5	Y
4	24	0.81	B	1.554 ±0.008	9.921 ±0.072	82.7	Y
5	“	“	“	1.51 ±0.010	9.928 ±0.035	85.0	N
6	“	“	“	1.485 ±0.014	9.896 ±0.051	86.7	Y
7	27	0.692	D (24), copper (3)	1.309 ±0.011	9.876 ±0.059	81.0	N
8	24	0.81	D (20), B (4)	1.551 ±0.022	9.921 ±0.056	82.8	Y
9	21	0.911	D	1.711 ±0.007	9.959 ±0.082	82.8	Y

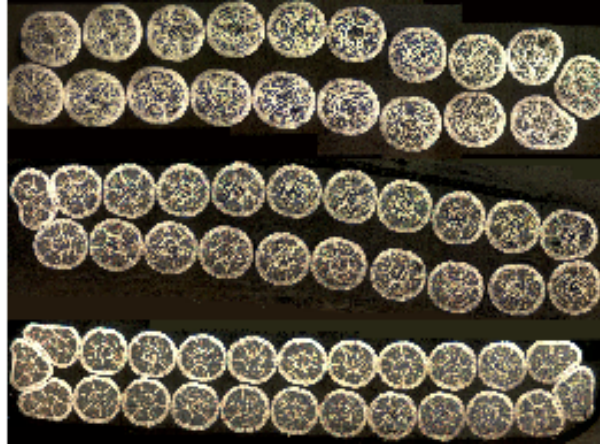


FIGURE 2. Cross section of 19-strand cable ID 1 (top), 21-strand cable ID 9 (middle), and 24-strand cable ID 4 (bottom).

Sample Preparation and Measurement Procedure

Virgin (round) strands, strands extracted from each cable and cable samples with welded ends were heat treated at OST in Oxygen atmosphere as shown in Figure 3. Critical current measurements were performed at Fermilab Superconductor R&D lab. Voltage-current (VI) characteristics were measured in boiling He at 4.2 K, in a transverse magnetic field, B , as described in [15]. The critical current I_c was determined using the $1 \mu\text{V}/\text{cm}$ criterion, with the usual measurement uncertainties [15]. Critical currents have not been corrected for self field effects which can be substantial at low fields. The cables were measured at self-field with a SC transformer equipped with a Rogowski coil to measure the secondary current [16].

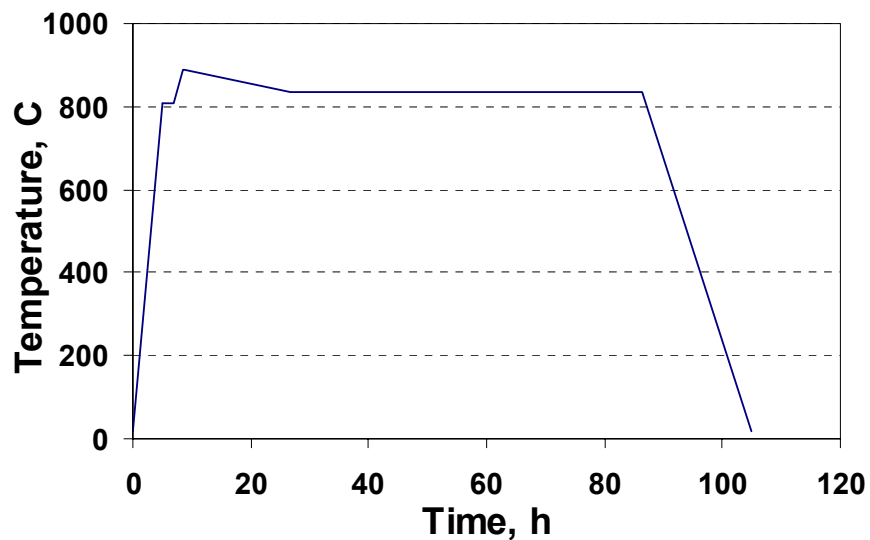


FIGURE 3. Optimized heat treatment schedule used for all the Bi samples.

RESULTS AND DISCUSSION

Round Strand

The maximum critical current density, J_c , that was obtained at 1 T and 12 T is shown as a function of size for strands C (regular O₂ anneal process) and D (modified process) in Figure 4. In this case, not much difference in J_c was found between the two different annealing processes used, but for strands of 0.81 mm. It is not clear why at 0.81 mm the J_c is reproducibly depressed in strand C.

Extracted Strand

Figure 5 (left) shows an example of V-I characteristics for a 0.91 mm round and extracted Bi-2212 strand (strand D from cable ID 9). At right the I_c at 4.2 K of these strands is shown as a function of field. The plot in Figure 6 of the normalized $I_c(4.2\text{ K})$ and that in Figure 7 of the normalized n-value, both as a function of cable packing factor, summarize the results obtained for all the extracted Bi-2212 strands. There is no noticeable dependence on magnetic field for either I_c or n-value. As can be seen, besides for one single case, which however was found to be reproducible, the I_c degradation of the extracted strands is reasonable and typically less than 20% at least up to 85% of packing factor. The n-value dependence with packing factor is stronger than for the I_c . Strands of different designs behave differently to cabling. For instance the I_c degradation is larger for strand B, which is an old design that had not been optimized for cabling.

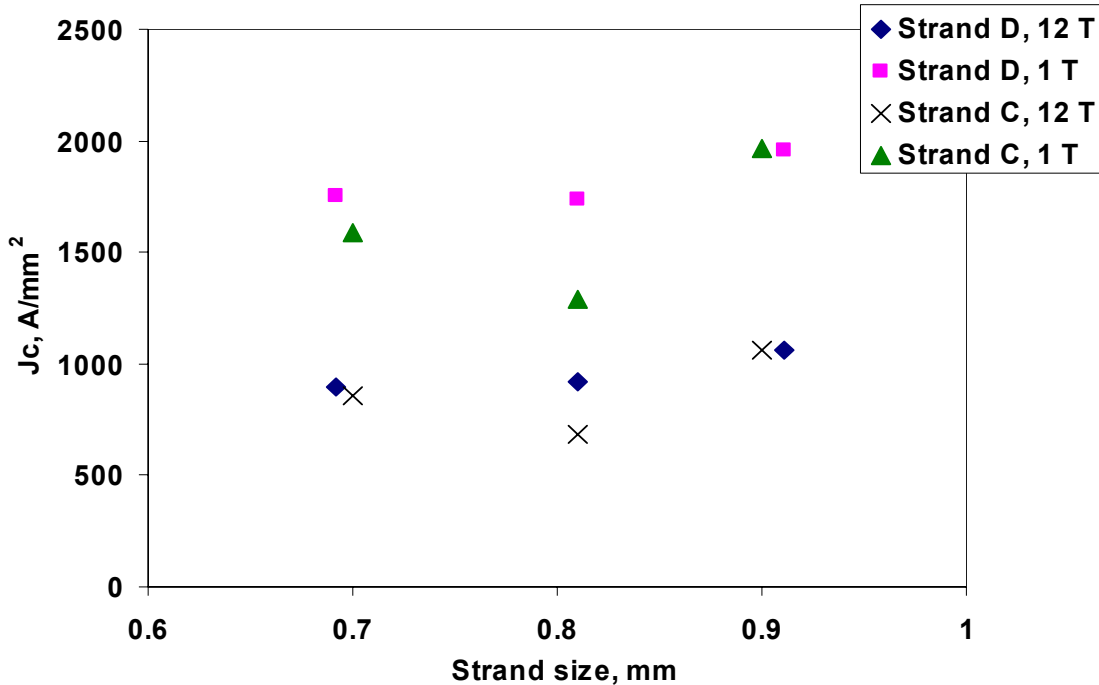


FIGURE 4. J_c at 4.2 K as a function of strand size for round strands C and D.

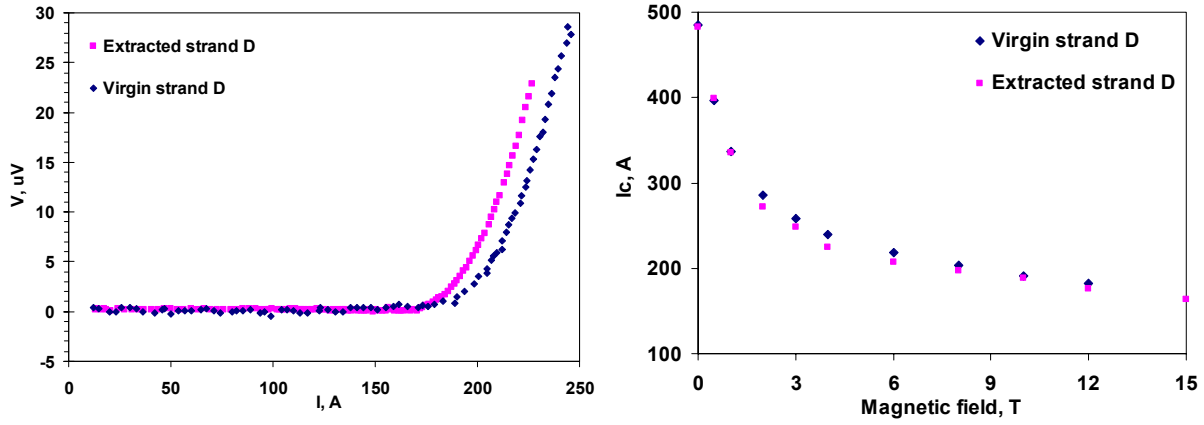


FIGURE 5. V-I curve at 12 T (left), and $I_c(4.2 \text{ K})$ as a function of field (right) for the 0.91 mm virgin and extracted Bi-2212 strand (strand D from cable ID 9).

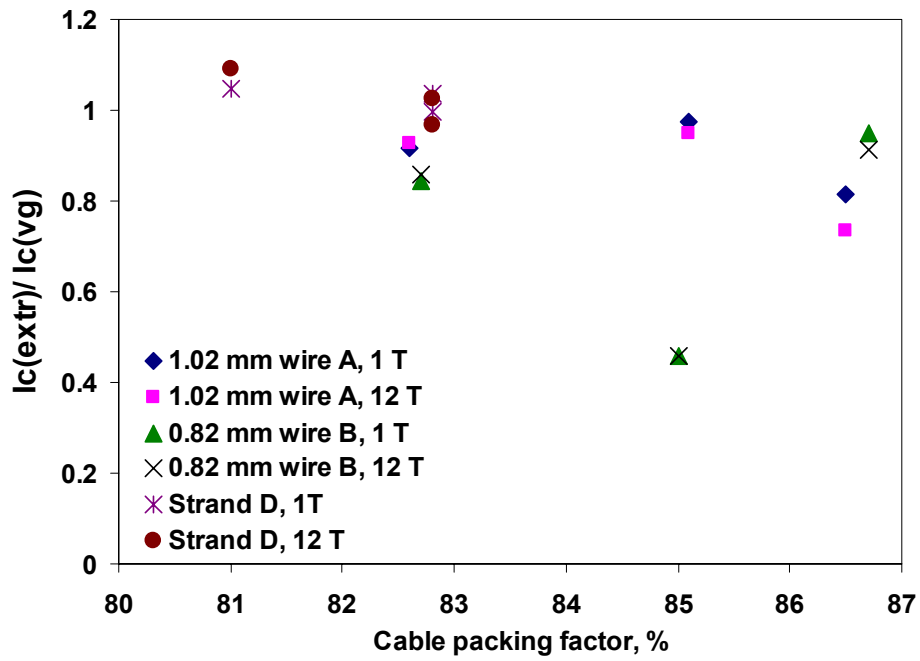


FIGURE 6. Normalized I_c at 4.2 K as a function of cable packing factor for the extracted Bi-2212 strands.

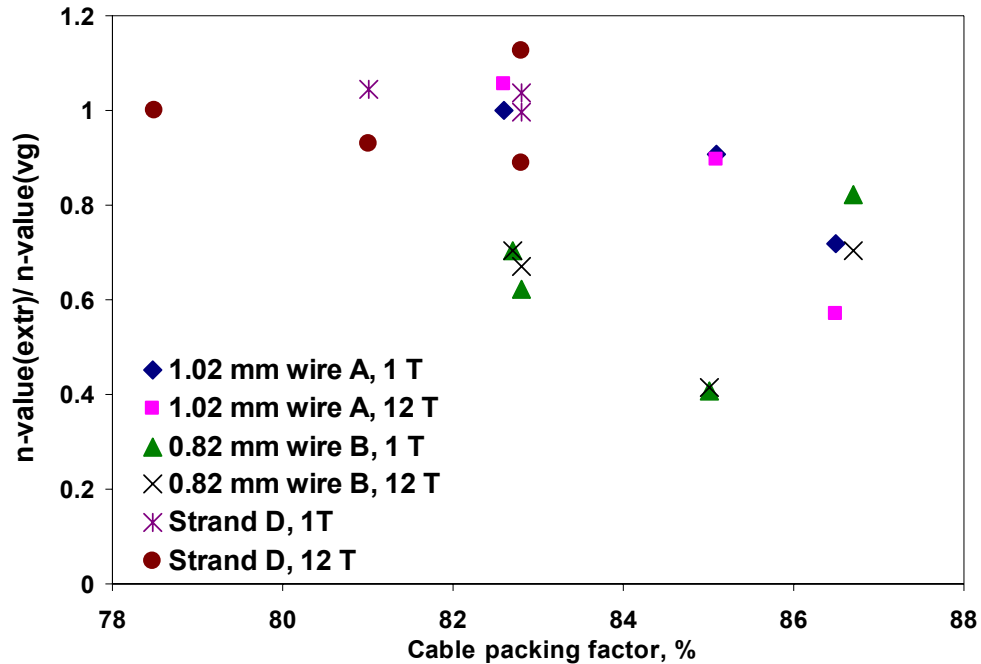


FIGURE 7. Normalized n-value at 4.2 K as a function of cable packing factor for the extracted Bi-2212 strands.

To better understand the behavior of the extracted strand with larger degradation (strand B from cable ID 5), SEM/EDS analysis was performed on the surface of tested samples of both this strand (Figure 8) and strand D from cable ID 9. It was found that both samples had MgO precipitates on the surface of the silver sheath consistently with its original Ag0.2%Mg alloy composition. However, the distribution density of the fine MgO precipitates in strand D was smaller than that in strand B (Figure 9). In addition, the EDS analysis revealed many abnormally large MgO precipitates in this strand, whereas strand D did not have any (Figure 10). These large precipitates may be caused by irregular grain growth, possibly due to heat treatment temperature inhomogeneities, but additional SEM studies of the cross section of the extracted strands should be performed to understand whether this effect is consistently reproducible.

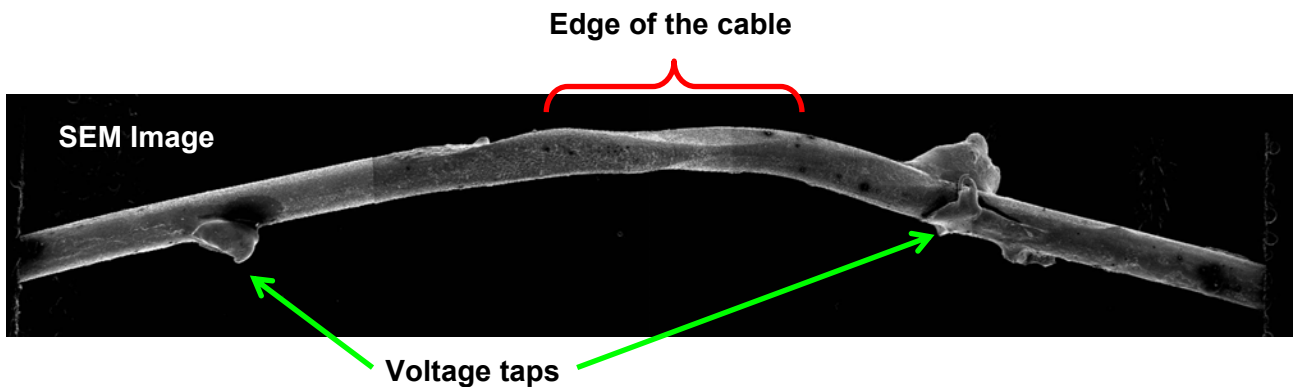


FIGURE 8. SEM image of tested sample of poorly performing strand B.

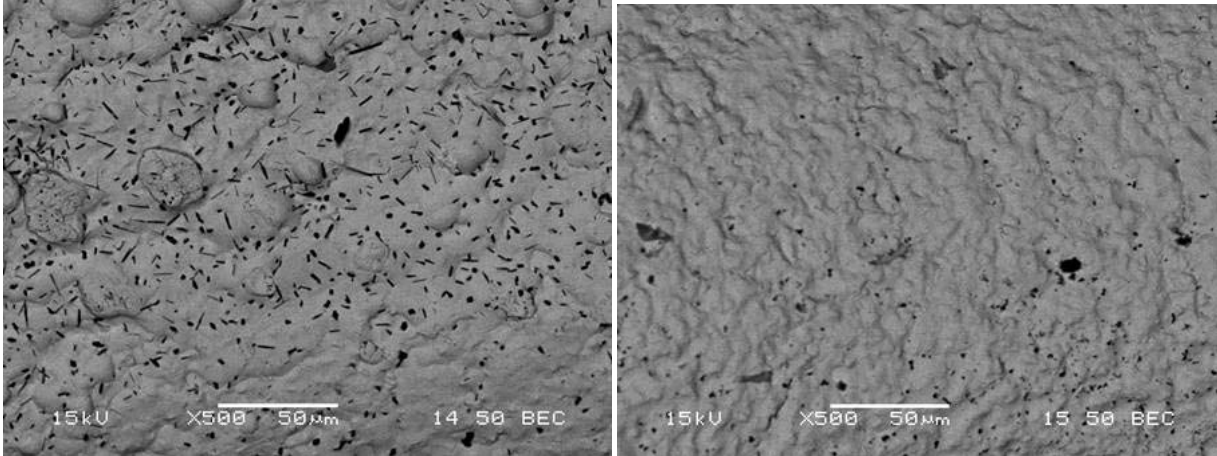


FIGURE 9. Distribution of the fine MgO precipitates in poorly performing strand B (left), and in good performance strand D (right).

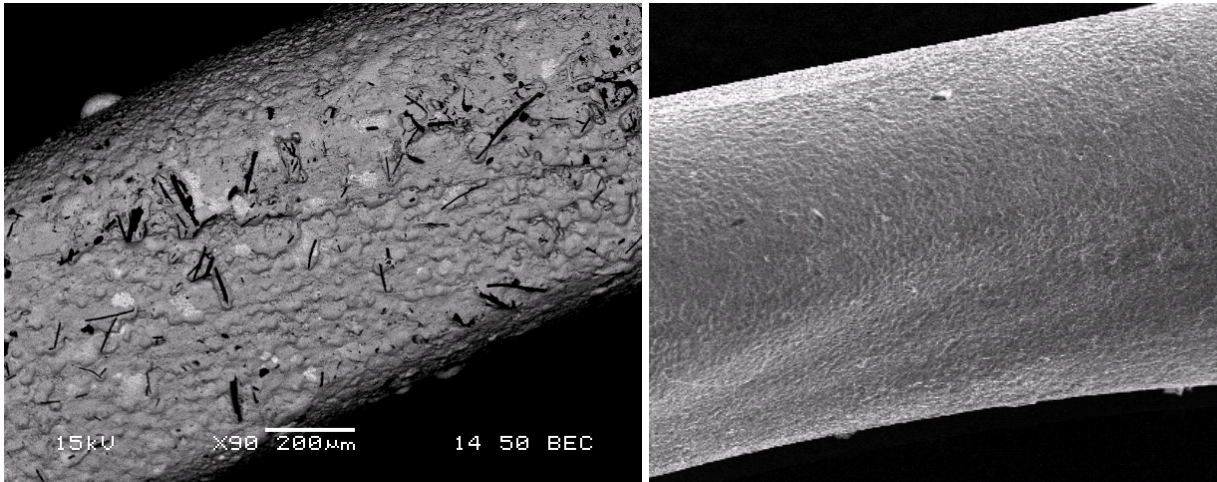


FIGURE 10. Abnormally large MgO precipitates in poorly performing strand B (left), and their absence in good performance strand D (right).

Cable Performance

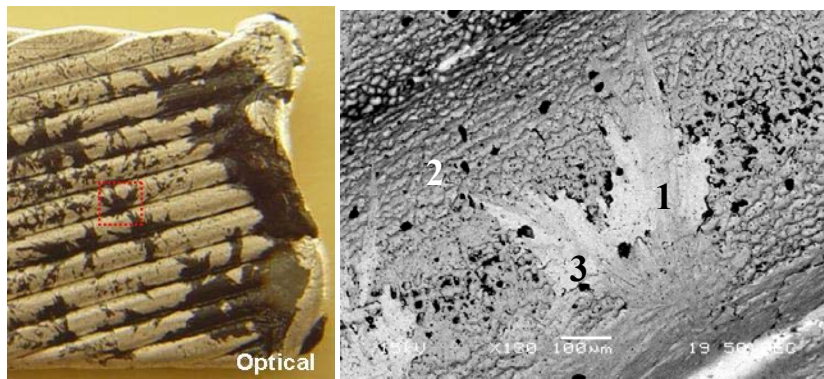
Table 3 shows the cable test results obtained at 4.2 K at self-fields of 0.1 to 0.3 T. For all the cables, an I_c degradation of about 50% was found. This current reduction on the cables was significantly and systematically larger than that of the extracted strands. To estimate the expected cable current, the average of the extracted strand critical currents at 0 T and 0.5 T was used, along with the cable strand composition in Table 2, because the self-field produced by the transformer secondary is 0.18 T to 0.29 T for cable currents between 3000 A and 5000 A. More accurate estimates could be performed in the future.

After reaction, the surface of all the cables showed black spots embedded in the silver coating as in Figure 11, left and center. SEM/EDS analysis performed on the surface of a cable showed that the composition of this black material was very close to that of Bi-2212 (Spectrum 1 in Table of Figure 11, at right), which must have come from the filament powder during heat treatment. In addition, a small crater was found at the edge of the sample. Analysis showed several oxide phases, with specific shapes and morphologies, such as Bi-2212 (needle like grains), Bi-2201 (step like

grains), (1,0) phase (spherical grains) and others. Further analysis would be needed to obtain more accurate chemical compositions, but it is already clear that the performance of these cables has been drastically degraded because of changes in the microstructure and chemical composition due to the powder leaks during heat treatment. However, because no leaks were observed either at the naked eye or through SEM on the extracted strands, which performed well, the hypothesis can be made that this problem is not as much related to the strand ability to withstand deformation as to the heat treatment of the cables itself, i.e. oxygen distribution on hidden surfaces, temperature inhomogeneities, and such.

TABLE 3. Cable Test Results

Cable ID	Impregnation	Bending	No. strands	Strand I_c (0 T)	Strand I_c (0.5 T)	Cable I_c (self-field)	Cable n-value	I_c (meas)/ I_c (exp)
1	Y	N	19	397	327	3617±35	8.8	53%
3	N	N	“	445	295	3743±51	10.1	53%
4	I	N	24	186	133	2251±27	10.1	59%
6	N	Y	“	216	148	1741±9	2.9	40%
8	N	Some	24	357, 217	289, 163	3229±16	5.9	44%
9	I	N	21	483	399	5188	-	56%



Spectrum No.	1	2	3
Element	At. %	At. %	At. %
Ag (L)	0	100	0
Bi (M)	14.91	0	3.59
Sr (L)	9.04	0	2.21
Ca (K)	5.53	0	0.78
Cu (L)	11.49	0	5.80
Mg (K)	0	0	29.33
O (K)	59.03	0	58.28
Totals	100.00	100.00	100.00

FIGURE 11. Bi-2212 cable after reaction (left), back scatter image of circled black spot (center), and composition Table in marked locations (right).

CONCLUSIONS

The focus of this work with OST was to produce Bi-2212 strands adequate for cabling. For this purpose, billets with different O_2 anneal processes were produced. These billets had very similar J_c 's. The I_c degradation of the extracted strands was reasonable and typically less than 20% at least up to 85% of packing factor for all the cables, but in one reproducible single case. It was found that the poorly performing strand had more and larger MgO precipitates on its surface than a well performing one. This may be caused by irregular grain growth, possibly due to heat treatment temperature inhomogeneities.

The I_c degradation measured on the cable samples was significantly and systematically larger than that of the extracted strands. It was found that this was due to changes in the microstructure and chemical composition due to powder leaks during heat treatment. However, because no leaks were observed on the extracted strands, which performed well, this problem may not be as much related to the strand ability to withstand deformation as to the heat treatment of the cables itself. Given the excellent performance of the Bi-2212 strands after cabling, it is worth to devote future resources to solve this cable heat treatment problem.

ANGULAR MEASUREMENTS OF HTS CRITICAL CURRENT FOR HIGH FIELD SOLENOIDS

First Generation (1G) multi-filamentary HTS are composites of silver or silver alloy matrix and BSCCO [17]. Second Generation (2G) HTS conductor is based on a thin film approach. Transverse cross sections of a 2G 344 coated conductor and a 1G Hermetic BSCCO-2223 tape are shown in Figure 10. 2G HTS wire is now seen as the major candidate for a lower cost HTS wire in the near future and an effective replacement for 1G HTS wire.

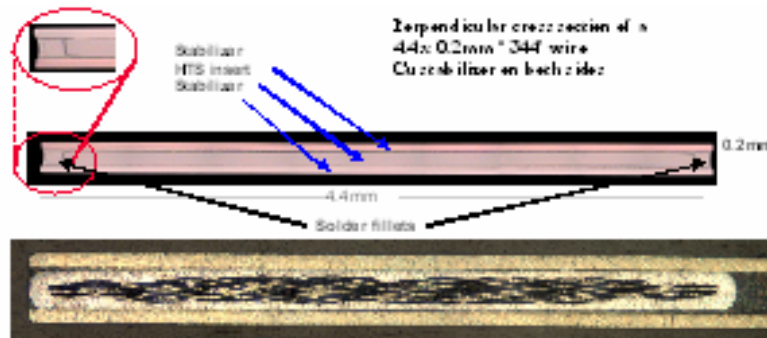


FIGURE 10. Transverse cross section of a 2G 344 coated conductor showing a YBCO layer 1 μm thick (top). Transverse cross section of a 1G Hermetic BSCCO-2223 tape showing 55 filaments of BSCCO-2223 embedded in a silver alloy matrix and 37 μm strips of stainless steel on top and bottom and solder fillets at the sides (bottom).

Both conductor types offer comparable electrical properties at lower temperatures. 2G becomes progressively superior to 1G when temperatures approach 77 K. 2G has excellent mechanical properties, and allows a react-and-wind technique for magnet construction.

The active component is the YBCO ($\text{YBa}_2\text{Cu}_3\text{O}_7$) or (RE)BCO layer, which is only around 1 μm thick. Despite the fact that only one such layer is present in a single conductor, the engineering critical currents are comparable to those of 1G wire. The corresponding critical current density in the YBCO layer is therefore very high ($>20 \text{ kA}/\text{mm}^2$ at 77 K, self-field), but this high J_c requires well-aligned YBCO grains. Typically, the YBCO grain boundary mis-orientation angle is below $3\text{--}4^\circ$, and the templates for growing these near-single crystal-like YBCO films are therefore well-textured. American Superconductor (AMSC) uses a bi-axially textured substrate approach onto which a thin epitaxial oxide buffer layer is deposited (RABiTSTM) [18, 19]. The epitaxial superconducting YBCO layer is grown using a low-cost, solution-based Metal Organic Deposition (MOD) process [20]. The coating processes allow a 40 mm or wider process width. After YBCO reaction and Ag coating the conductor is slit to near-final conductor width, typically 4 mm [21, 22]. This slit “insert” conductor is then laminated on both sides to a slightly wider (4.4 mm) foil, which can consist of different materials. Copper laminates are used for coil and cable applications; stainless laminates are used for fault current limiters. This 3-ply geometry is now sold by AMSC as “344” superconductors. The “3” indicates the 3-ply geometry and 44 the 4.4 mm width. The laminate provides mechanical, electrical and thermal stability and facilitates a robust winding process for coil applications. AMSC also developed a slightly wider conductor, the so-called 348 superconductor (4.8 mm wide). This wider superconductor was used for this work.

BSCCO-2223 and 2G HTS are typically produced in the form of tapes, which are anisotropic and exhibit the highest critical current when the magnetic field is applied parallel to the tape face

(B_{PAR}) and the lowest one when the field is perpendicular (B_{PERP}). Figure 11 shows the geometrical configuration of a tape and relative directions of magnetic field.

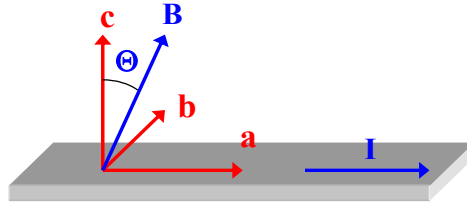


FIGURE 11. HTS superconductor with current direction and relative direction of magnetic field B. B is always perpendicular to the current direction.

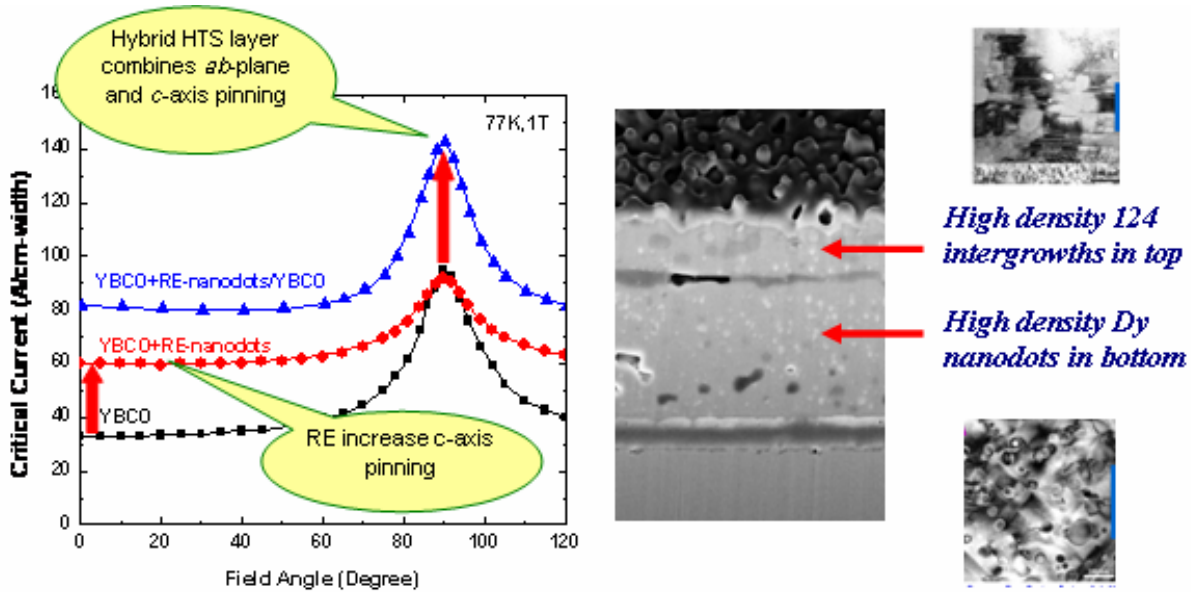


FIGURE 12. Field-angle dependence of $I_c(77K, 1T)$ in a conductor with a 1.4 μm thick hybrid layer (left). At right, top layer is undoped YBCO with planar defects, bottom layer is doped with RE oxide for c-axis pinning.

Flux pinning in YBCO can be strongly influenced by additions of rare earth oxides, in particular when they segregate as small particles (“nanodots”) which tend to enhance pinning for field orientations perpendicular to the YBCO film plane [22, 23]. Stacking faults are very effective in enhancing pinning for field orientations parallel to the film plane. To use the advantages of both pinning mechanisms a Double Layer Hybrid was developed. An example is shown in Figure 12 at right [22], where nanodots (see bottom TEM image) enhance the perpendicular-field I_c values and the planar 124 stacking faults (top TEM image) maintain effective ab-plane pinning. Figure 3 (left) also shows that at 77 K, 1 T the performance of this new conductor using this hybrid YBCO layer, approximately 1.4 μm thick, is enhanced over the entire angular range.

Earlier BSCCO tapes have been tested at various temperatures in both field directions [24]. Angular measurements on PLD and MOD YBCO have mainly focused on higher temperatures [25]. In this study we were interested in the capabilities of both superconductors for potential high field solenoids, suitable for future Muon Collider systems, and for this application, the choice in temperature ranged from 1.8 K to 33 K, at magnetic fields up to 15 T. We also measured the magnetic field dependence as a function of magnetic field angle Θ .

EXPERIMENTAL SETUP

Samples Description

A BSCCO-2223 Hermetic tape and a 2G 348 Coated conductor produced by AMSC were tested. Samples specifications are given in Table 4.

TABLE 4. HTS Specifications (2G HTS performance for this study slightly higher than quoted 110A)

	Hermetic BSCCO-2223 tape	348 Superconductor
Min I_c (77 K, self-field, 1 μ V/cm)	115 A	110 A
Average thickness t_T	0.31 mm	0.2 mm
Average width w_T	4.8 mm	4.8 mm
Laminate	stainless	copper
Laminate thickness	2 x 0.037 mm	2 x 0.050 mm
YBCO layer thickness		1.4 μ m
Min. critical bend diameter	50 mm	50 mm
Max. rated tensile strain (95% I_c retention)	0.3 %	0.3 %

Sample Holders

Samples were 38 mm long. Figure 13 shows the sample holder that was designed and used to change the direction of the c-axis of the tape with respect to the external magnetic field. The sample, supported in its middle part by G-10, was soldered within a groove on two Cu half cylinders (Figure 4, left). A splice length of 12 mm was used on each side of the sample to control contact resistance and heating power. The sample holder was placed at the desired angle within cylindrical holes in the probe Cu lugs (Figure 4, center). To provide electrical contact the lugs were then tightened using stainless steel screws. Current transfer length requirements determined the distance between the voltage taps, which was of 10 mm (Figure 4, right).

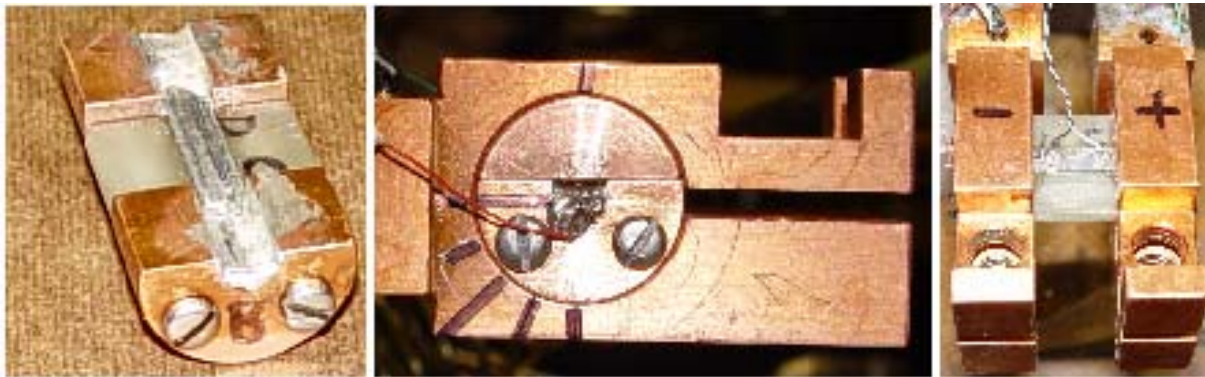


FIGURE 13. Sample holder (left), sample holder within the probe copper lugs (center), and instrumented sample (right).

Measurement Procedure

Critical current measurements were performed at Fermilab Superconductor R&D lab. Measurements were obtained at the various temperatures in a Variable Temperature Insert (VTI)

with an inner diameter of 49 mm, within a 15/17 T magneto-cryostat. The current was provided to the sample using 2000 A current leads. The angle Θ was changed in steps of 11.25° and 22.5° . First, critical current measurements were performed in liquid nitrogen (77 K) in self-field. Next, voltage-current (VI) characteristics were measured in He (liquid or vapor) at a magnetic field between 0 and 15 T. The critical current I_c was determined using the $1 \mu\text{V}/\text{cm}$ criterion, with the usual measurement uncertainties [15]. Critical currents have not been corrected for self field effects which can be substantial at low fields.

RESULTS AND DISCUSSION

BSCCO-2223 Hermetic Wire

Figure 14 shows I_c results as a function of magnetic field for the BSCCO-2223 tape, in the parallel and transverse field configurations, from 1.8 K to 33 K. The I_c test results in nitrogen at 77 K were 122 ± 1 A. The I_c performance at 1.8 K was more than 10% better up to 15 T. It is also worth noting that these hermetic tapes were able to perform without any degradation after several thermal cycles.

To gauge field and temperature dependence of the anisotropy, the ratio of I_c , normalized to $I_c(77 \text{ K}, 0 \text{ T})$, in parallel field to that in transverse field as a function of applied magnetic field at the various temperatures is plotted in Figure 15. One can see that this ratio depends on both field and temperature. The field dependence is consistent with a linear one, where the slope value increases with temperature.

Figures 16 and 17 show the angular dependence. The I_c normalized to $I_c(77 \text{ K}, 0 \text{ T})$ as a function of the field angle at various magnetic fields is plotted at 4.2 K and 33 K. The data taken at 0 T field are shown as representative of the measurement uncertainty. Most of the I_c reduction occurs between 90 and 45 degree.

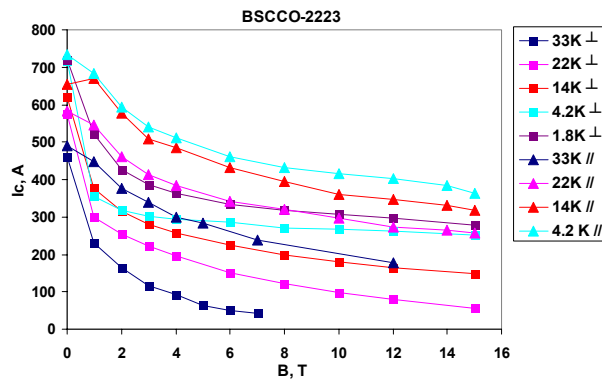


FIGURE 14. $I_c(B, T)$ of the Bi-2223 hermetic wire in parallel and perpendicular fields, 1.8-33 K.

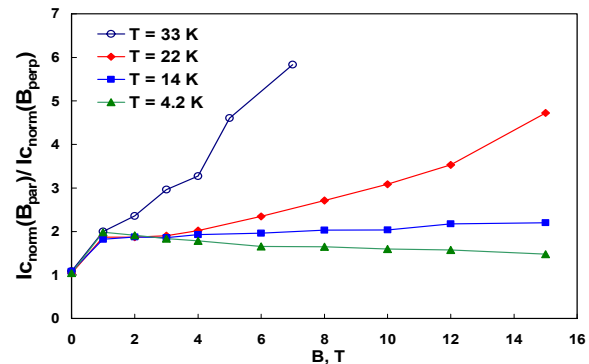


FIGURE 15. Ratio of normalized I_c in parallel and perpendicular fields, 4.2-33 K, for the Bi-2223.

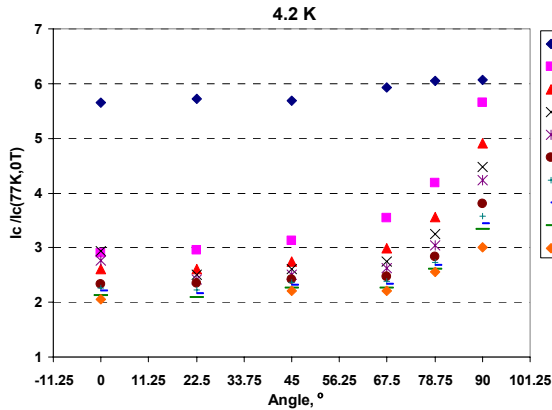


FIGURE 16. Normalized $I_c(4.2\text{ K})$ of the Bi-2223 hermetic conductor versus B and Θ .

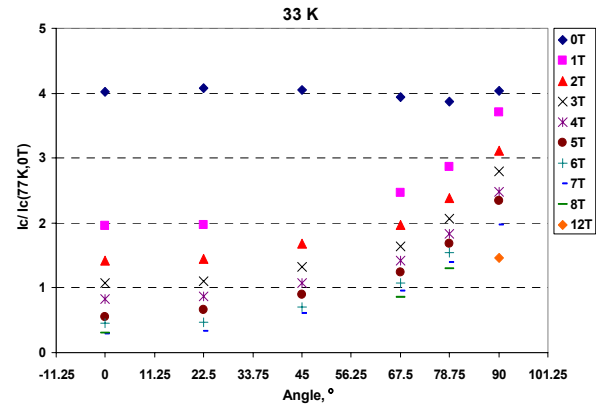


FIGURE 17. Normalized $I_c(33\text{ K})$ of the Bi-2223 hermetic conductor versus B and Θ .

2G 348 Coated Conductor

Figure 18 shows I_c results as a function of magnetic field for the 2G 348 conductor, in the parallel and transverse field configurations, from 4.2 K to 33 K. The performance at self-field and 77 K was 127 A for the sample tested in parallel configuration and 153 A for that used in the transverse configuration. One can see that the I_c dependence in parallel field for the 2G 248 reduces mostly linearly with field, which indicates that effective pinning is maintained for the parallel direction over the entire field range; for the perpendicular direction pinning is most effective at low fields but then reduces at high fields.

Figure 19 shows the ratio of I_c , normalized to $I_c(77\text{ K}, 0\text{ T})$, in parallel field to that in transverse field as a function of applied magnetic field at the various temperatures. Contrary to the 1G conductor, in this case there is no observable temperature dependence. The ratio tends to saturate at high fields, at around 7.

Figures 20 and 21 show the I_c normalized to $I_c(77\text{ K}, 0\text{ T})$ as a function of field and field angle at 4.2 K and 33 K. Also for the 2G, most of the I_c reduction occurs between 90 and 45 degree, with a possible indication of a more gradual reduction with angle at 4.2 K, but more data would be needed to confirm this.

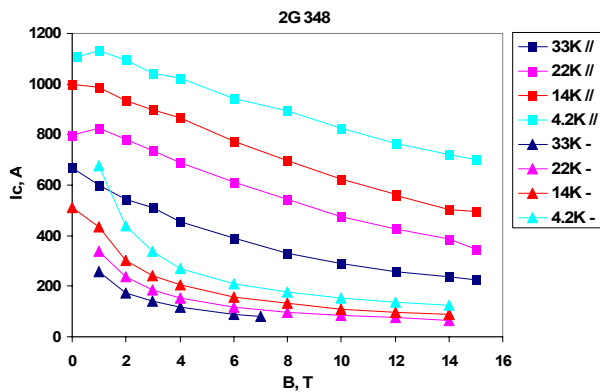


FIGURE 18. $I_c(B,T)$ of the hybrid 2G 348 in parallel and perpendicular fields, 4.2-33 K.

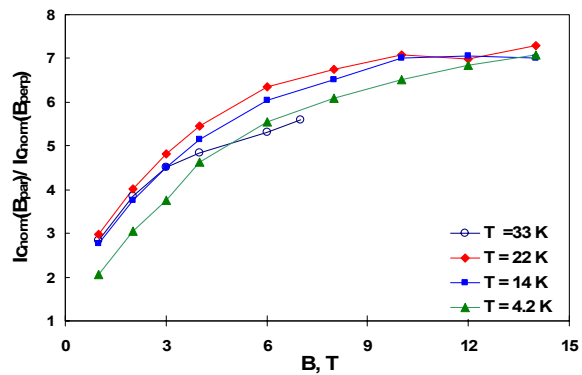


FIGURE 19. Ratio of normalized I_c in parallel and perpendicular fields, 4.2-33 K, for the 2G 348.

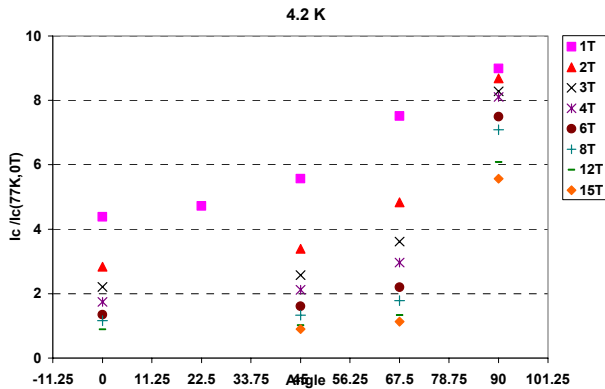


FIGURE 20. Normalized $I_c(4.2\text{ K})$ of the 2G coated conductor versus B and Θ .

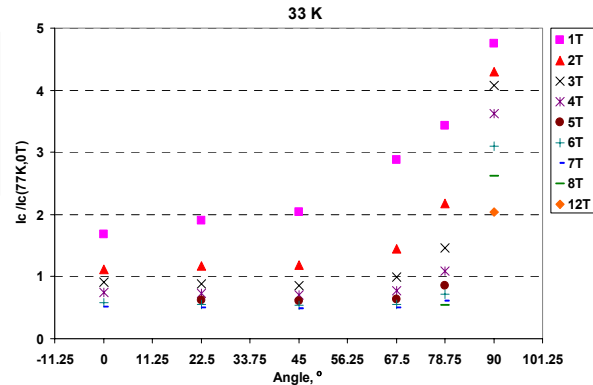


FIGURE 21. Normalized $I_c(33\text{ K})$ of the 2G coated conductor versus B and Θ .

Comparison with Low Temperature Superconductors

Figure 22 shows the engineering critical current J_E at 4.2 K and magnetic fields up to 15 T, for 2G 348 and Bi-2223 superconductors, and round Bi-2212 (OST), Nb_3Sn and $NbTi$ wires. For the calculation of J_E of the 2G 348 conductor the entire cross section was used. Below 15 T, the J_E of the RPP Nb_3Sn wire exceeds that of all HTS at 4.2 K. Above 17 T the Bi-2212 conductor shows an excellent overall performance. The 348 superconductors show a much higher current density in parallel fields, indicating excellent potential for high current density insert magnets for very high fields. For complete solenoids in which end sections operate with high perpendicular field components the B_{perp} performance is currently too low and needs further pinning enhancement for this field direction. The Bi-2223 conductor shows a lower engineering critical current density than either Bi-2212 or 348, but combines high strength, react and wind capability, and low angular field dependence of J_c .

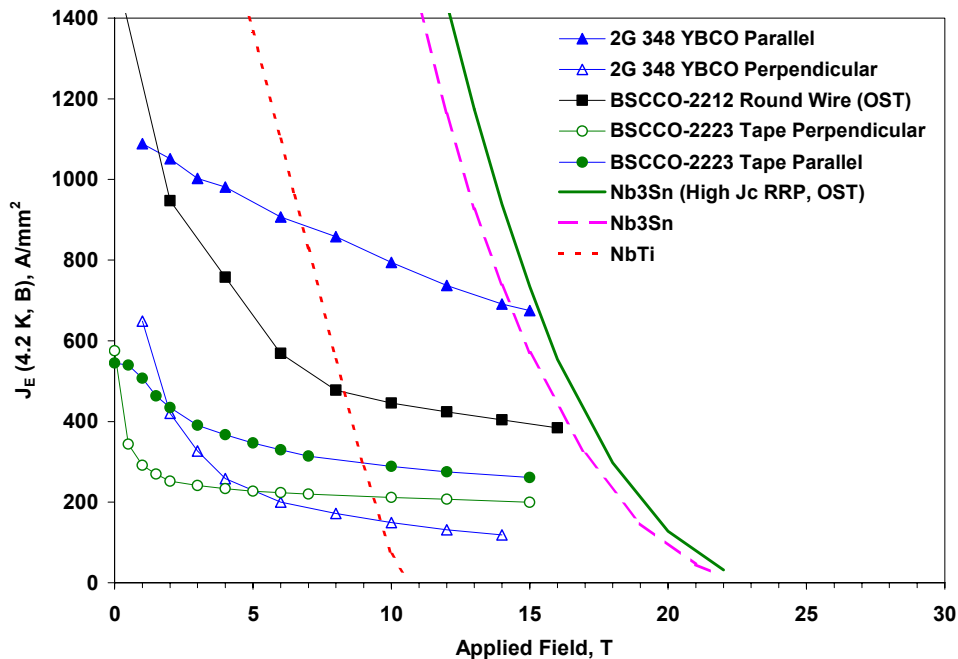


FIGURE 22. $J_E(B)$ at 4.2 K for 348 superconductors, Bi-2223 wire, round Bi-2212 wire (OST), and high current density Nb_3Sn wire.

CONCLUSIONS

A major challenge for BSCCO-2212 are the powder leaks when heat treating cable. Given the excellent performance of the Bi-2212 OST strands after cabling, it is worth to devote future resources to solve this cable heat treatment problem.

A sample holder was designed to perform I_c measurements of HTS tapes under externally applied magnetic fields, with orientations varying from zero to 90 degree with respect to the c-axis. This was performed from 1.8 K to 33 K up to 15 T, while providing up to 1200 A of current. The data are consistent with similar measurements performed by AMSC in a perpendicular field at 4.2 K [18]. The engineering critical current for the new double layer hybrid 2G HTS superconductor competes well with existing conductors for parallel field orientations. With further c-axis pinning development, it is an excellent candidate for high field insert magnets operating above 16-18 T.

For the design of high field solenoids, measurements at 4.2 K and at fields greater than 15 T should be addressed for the future, as well as axial strain dependence [26, 27].

ACKNOWLEDGMENTS

We thank the special people of our Superconductor R&D group at FNAL, Al Rusy, Tom VanRaes and Marianne Bossert, whose skills and commitment were essential for this work.

REFERENCES

1. U.S. National Research Council's Committee on Opportunities in High Magnetic Field Science, "Opportunities in High Magnetic Field Science", National Academies Press, Washington, D.C., 2005.
2. A. Street, "Superconducting magnets: at the heart of NMR", *Spectroscopy Europe*, vol. 15, no. 1, pp. 10-13, 2003.
3. S.W. Van Sciver and K.R. Marken, "Superconducting magnets above 20 tesla", *Physics Today*, vol. 55, no. 8, pp. 37-44.
4. Oxford Instruments Superconductivity, "Oxford Instruments announces the world's first 950 MHz magnet for Nuclear Magnetic Resonance is at field", press release, August 31, 2005.
5. S. Hong, M.B. Field, J.A. Parrell and Y. Zhang, "Latest improvements of current-carrying capability of Nb-Sn", *IEEE Trans. Appl. Sup. (MT-19)*.
6. E. Barzi et al., "BSCCO-2212 Wire and Cable Studies", submitted to CEC/ ICMC 2007.
7. D. Turrioni et al., "Angular Measurements of HTS Critical Current for High Field Solenoids", submitted to CEC/ ICMC 2007.
8. H. Miao, K.R. Marken, M. Meinesz, B. Czabaj and S. Hong, "Development of Round Multifilament Bi-2212/Ag Wires for high Field Magnet Applications", *IEEE Trans. Appl. Sup.*, vol. 15, p. 2554, 2005.
9. T. Hasegawa, T. Koizumi, Y. Hikichi, T. Nakatsu, R. Scanlan, N. Hirano and S. Nagaya, "HTS conductors for magnets", *IEEE Trans. Appl. Sup.*, vol. 12, p. 1136, 2002.
10. T. Hasegawa, N. Ohtani, T. Koizumi, Y. Aoki, S. Nagaya, N. Hirani, L. Motowidlo, R.S. Sokolowski, R.M. Scanlan, D.R. Dietderich, and S. Hanai, "Improvement of Superconducting Properties of Bi-2212 Round Wire and Primary Test Results of Large Capacity Rutherford Cable", *IEEE Trans. Appl. Sup.*, vol. 11, p. 3034, 2001.
11. T. Hasegawa, J. Nishioka, N. Ohtani, Y. Hikichi, R. Scanlan, R. Gupta, N. Hirano and S. Nagaya, "12 kA HTS Rutherford Cable", *IEEE Trans. Appl. Sup.*, vol. 14, p. 1066, 2004".
12. R.M. Scanlan, D.R. Dietderich, H.C. Higley, K.R. Marken, L.R. Motowidlo, R. Sokolowski, and T. Hasegawa "Fabrication and Test Results for Rutherford-type Cables Made from BSCCO Strands", *IEEE Trans. Appl. Sup.*, vol. 9, p. 130, 1999.
13. H. Miao, K.R. Marken, M. Meinesz, B. Czabaj and S. Hong, "Development of Bi-2212 Conductors for Magnet Applications", *Adv. Cryog. Eng.*, vol. 50, p. 603, 2004.

14. N. Andreev et al., "Development of Rutherford-type Cables for High Field Accelerator Magnets at Fermilab", Applied Superconductivity Conference, Aug. 27-Sep. 1, 2006, Seattle, WA. Paper accepted in IEEE Trans. Appl. Sup.
15. E. Barzi et al., "High Temperature Superconductors for High Field Superconducting Magnets", Advances in Cryogenic Engineering, V. 52, p. 416, 2006.
16. D. Turrioni et al., "Study of Nb₃Sn Cable Stability at Self-field using a SC Transformer", IEEE Trans. Appl. Sup., V. 15, No. 2, June 2005, p. 1537.
17. Goyal, D.P. Norton, J.D. Budai, M. Paranthaman, E.D. Specht, D.M. Kroeger, D.K. Christen, Q. He, B. Saffian, F.A. List, D.F. Lee, P. M. Martin, C.E. Klabunde, E. Hardtfield, and V.K. Sikka, Appl. Phys. Lett. 69, 1975 (1996).
18. C.L.H. Thieme, S. Annavarapu, W. Zhang, V. Prunier, L. Fritzemeier, Q. Li, U. Schoop, M.W. Rupich, M. Gopal, S. Foltyn and T. Holesinger., "Non-magnetic Substrates for Low Cost YBCO Coated Conductors", IEEE Trans. Appl. Superc. 11, p. 3329 (2001).
19. X. Li^a, M.W. Rupich, T. Kodenkandath, Y. Huang, W. Zhang, E. Siegal, D. T. Verebelyi, U. Schoop, N. Nguyen, C. Thieme, Z. Chen, D.M. Feldman, D. C. Larbalestier, T.G. Holesinger, L. Civale, X. Jia, V. Maroni, and M.V. Rane, "High Critical Current YBCO Films Prepared by an MOD Process on RABiTS Templates", to appear in IEEE Trans. Appl. Superc. 17 (2007).
20. M. W. Rupich, U. Schoop, D. T. Verebelyi, C. Thieme, W. Zhang, X. Li, T. Kodenkandath, N. Nguyen, E. Siegal, D. Buczek, J. Lynch, M. Jowett, E. Thompson, J-S. Wang, J. Scudiere, A. P. Malozemoff, Q. Li, S. Annavarapu, S. Cui, L. Fritzemeier, B. Aldrich, C. Craven, F. Niu, A. Goyal, and M. Paranthaman, "YBCO Coated Conductors, IEEE Trans. Appl. Superc. 13, p. 2458 (2003).
21. M. W. Rupich, U. Schoop, C. Thieme, D. T. Verebelyi, W. Zhang, X. Li, T. Kodenkandath, N. Nguyen, E. Siegal, L. Civale, T. Holesinger, A. Goyal, and M. Paranthaman, "Second Generation HTS Wire Based on RABiTSTM Substrates and MOD YBCO", IEEE Trans. Appl. Superc. 15, p. 2458 (2005).
22. M.W. Rupich, U. Schoop, D.T. Verebelyi, C.L.H. Thieme, D. Buczek, X. Li, W. Zhang, T. Kodenkandath, Y. Huang, E. Siegal, W. Carter, N. Nguyen, J. Schreiber, M. Prasova, J. Lynch, D. Tucker, R. Harnois, C. King, D. Aized, "The Development of Second Generation HTS Wire at American Superconductor", to appear in IEEE Trans. Appl. Superc. 17 (2007).
23. W. Zhang, Y. Huang, X. Li, T. Kodenkandath, M.W. Rupich, U. Schoop, D.T. Verebelyi, C.L.H. Thieme, E. Siegal, T.G. Holesinger, B. Maiorov, L. Civale, D.J. Miller, V.A. Maroni, J. Li, P.M. Martin, E.D. Specht, A. Goyal and M.P. Paranthaman, "Control of Flux Pinning in MOD YBCO Coated Conductor," to appear in IEEE Trans. Appl. Superc. 17 (2007).
24. B. Xu, J.H. Su and J. Schwartz, "Dependence of transport critical current of magnetic field processed Bi₂Sr₂CaCu₂O_x/AgMg tapes on the background magnetic field and magnetic field direction," *Superconductor Science and Technology* **18** 503-507 (2005).
25. T. Holesinger and L. Civale, "Multi-scale Characterization of Structure and Properties of Coated Conductors", DOE Superconductivity for Electric Systems 2006 Annual Peer Review, August 2006, Washington, D.C.
26. J. Ekin, N. Cheggour, DOE Superconductivity for Electric Systems 2004 Annual Peer Review, July 2004, Washington, D.C.
27. D Uglietti, B Seeber, V Abächerli, W L Carter and R Flükiger, "Critical currents versus applied strain for industrial Y-123 coated conductors at various temperatures and magnetic fields up to 19 T", Supercond. Sci. Technol. **19** No 8 (August 2006) 869-872.